THE JOURNAL OF BIOLOGICAL CHEMISTRY VOL. 281, NO. 39, pp. 29030–29041, September 29, 2006

Denmotoxin, a Three-finger Toxin from the Colubrid Snake *Boiga dendrophila* (Mangrove Catsnake) with Bird-specific Activity*

Received for publication, June 19, 2006, and in revised form, July 21, 2006 Published, JBC Papers in Press, July 24, 2006, DOI 10.1074/jbc.M605850200

Joanna Pawlak[‡], Stephen P. Mackessy[§], Bryan G. Fry[‡1], Madhav Bhatia[¶], Gilles Mourier[‖], Carole Fruchart-Gaillard[‖], Denis Servent[‖], Renée Ménez[‖], Enrico Stura[‖], André Ménez[‖], and R. Manjunatha Kini[‡2]**

*From the [‡]Department of Biological Sciences, Faculty of Science, and the [¶]Department of Pharmacology, Faculty of Medicine, National University of Singapore, Singapore 117543, the [§]School of Biological Sciences, University of Northern Colorado, Greeley, Colorado 80639-0017, the [‖]Département d'Ingénierie et d'Etudes des Protéines, Commissariat à l'Energie Atomique, Gif-sur-Yvette Cedex 91191, France, and the **Department of Biochemistry and Molecular Biophysics, Medical College of Virginia, Virginia Commonwealth University, Richmond, Virginia 23298*

Boiga dendrophila **(mangrove catsnake) is a colubrid snake that lives in Southeast Asian lowland rainforests and mangrove swamps and that preys primarily on birds. We have isolated, purified, and sequenced a novel toxin from its venom, which we named denmotoxin. It is a monomeric polypeptide of 77 amino acid residues with five disulfide bridges. In organ bath experiments, it displayed potent postsynaptic neuromuscular activity and irreversibly inhibited indirectly stimulated twitches in chick biventer cervicis nerve-muscle preparations. In contrast, it induced much smaller and readily reversible inhibition of electrically induced twitches in mouse hemidiaphragm nerve-muscle preparations. More precisely, the chick muscle $\alpha_1\beta\gamma\delta$-nicotinic acetylcholine receptor was 100-fold more susceptible compared with the mouse receptor. These data indicate that denmotoxin has a bird-specific postsynaptic activity. We chemically synthesized denmotoxin, crystallized it, and solved its crystal structure at 1.9 Å by the molecular replacement method. The toxin structure adopts a non-conventional three-finger fold with an additional (fifth) disulfide bond in the first loop and seven additional residues at its N terminus, which is blocked by a pyroglutamic acid residue. This is the first crystal structure of a three-finger toxin from colubrid snake venom and the first fully characterized bird-specific toxin. Denmotoxin illustrates the relationship between toxin specificity and the primary prey type that constitutes the snake's diet.**

Three-finger toxins (3FTXs)[3] form one of the most abundant, well recognized families of snake venom proteins. They share a similar structure and are characterized by three β-stranded finger-like loops, emerging from a globular core and stabilized by four conserved disulfide bridges. An additional disulfide linkage may sometimes be present in the first (non-conventional toxins) or second (long-chain α-neurotoxins and κ-toxins) loop (1–5). All 3FTXs are monomers except for κ-toxins, which are noncovalent homodimers isolated from *Bungarus* venoms. Minor structural differences in the three-finger fold, *viz.* the number of β-strands, overall morphology of the loops, and differential lengths of turns or C-terminal tails (6), lead to the recognition of varied targets and modulate the toxicity and specificity (7). Hence, 3FTXs affect a broad range of molecular targets, including α_1-nicotinic acetylcholine receptors (nAChRs; short- and long-chain α-neurotoxins), α_7-nAChRs (long-chain α-neurotoxins), and α_3- and α_4-nAChRs (κ-toxins) (4, 5); muscarinic acetylcholine receptors (muscarinic toxins) (8); L-type calcium channels (calciseptine and FS2 toxin) (9, 10); integrin $\alpha_{IIb}\beta_3$ (dendroaspin) (11, 12); integrin $\alpha_v\beta_3$ (cardiotoxin A5) (13); acetylcholinesterase (fasciculins) (14); phospholipids and glycosphingolipids (cardiotoxins) (15); and blood coagulation protein factor VIIa (16). As the interaction with such a broad spectrum of target proteins results in a variety of pharmacological effects, the understanding of the physiological role and mechanism of action supported by the architecture of 3FTXs could be of great value in the development of novel research tools or rational drug design. For instance, studies with α-bungarotoxin led to a detailed characterization of muscle nAChR, helping to elucidate the fundamental underlying mechanisms involved in neuromuscular transmissions (17).

3FTXs were thought to occur only in the venoms of the snake family Elapidae. But recently, our laboratory reported the first

* This work was supported by a Biomedical Research Council grant from the Agency for Science, Technology and Research, Singapore. The costs of publication of this article were defrayed in part by the payment of page charges. This article must therefore be hereby marked "*advertisement*" in accordance with 18 U.S.C. Section 1734 solely to indicate this fact.

The atomic coordinates and structure factors (code 2H5F) have been deposited in the Protein Data Bank, Research Collaboratory for Structural Bioinformatics, Rutgers University, New Brunswick, NJ (http://www.rcsb.org/).

The nucleotide sequence(s) reported in this paper has been submitted to the DDBJ/GenBank™/EBI Data Bank with accession number(s) DQ366293.

[1] Present address: Australian Venom Research Unit, School of Medicine, University of Melbourne, Parkville, Victoria 3010, Australia.

[2] To whom correspondence should be addressed: Protein Science Lab., Dept. of Biological Sciences, Faculty of Science, National University of Singapore, Science Dr. 4, Singapore 117543. Tel.: 65-6516-5235; Fax: 65-6779-2486; E-mail: dbskinim@nus.edu.sg.

[3] The abbreviations used are: 3FTXs, three-finger toxins; nAChRs, nicotinic acetylcholine receptors; RP-HPLC, reversed-phase high pressure liquid chromatography; RT, reverse transcription; Fmoc, *N*-(9-fluorenyl)methoxycarbonyl; CBCM, chick biventer cervicis muscle; MHD, mouse hemidiaphragm muscle; ESI/MS, electrospray ionization mass spectrometry; AChBP, acetylcholine-binding protein.

colubrid snake venom toxin (α-colubritoxin from *Coelognathus radiatus*), a reversible antagonist of chick muscle nAChRs (18). The large polyphyletic family Colubridae consists of approximately two-thirds of the described species of the advanced snakes and includes >700 different venomous species (19, 20). Colubrid snakes possess a venom gland (the Duvernoy's gland) with a common duct extending to the posterior lingual region of the maxilla, commonly associated with grooved or enlarged posterior maxillary teeth. Relatively little is known of the chemistry, toxicology, and immunology of colubrid venoms, and a more thorough investigation of colubrid venom components holds great promise for discovering new bioactive compounds (21, 22).

In this work, we report the isolation, purification, and pharmacological and structural characterization of a novel bird-specific neurotoxin, denmotoxin, one of the major venom components of the mangrove catsnake (*Boiga dendrophila*). Denmotoxin produced a virtually irreversible blockage of chick muscle $\alpha_1\beta\gamma\delta$-nAChRs, whereas it produced a much weaker, readily reversible blockage of mouse muscle $\alpha_1\beta\gamma\delta$-nAChRs. In addition to pharmacological and biochemical studies, we have established a chemical synthesis and refolding protocol for synthetic denmotoxin and solved the high resolution crystal structure of the protein. Denmotoxin has great potential to become a model for a better understanding of the mechanisms of species specificity as well as reversible binding of venom neurotoxins.

EXPERIMENTAL PROCEDURES

Materials—Most chemicals and drugs (including carbamylcholine chloride, *d*-tubocurarine chloride, and neostigmine bromide) were purchased from Sigma. Trypsin and Lys-C endopeptidase were purchased from Wako Pure Chemicals (Osaka, Japan), and *Pfu* pyroglutamate aminopeptidase was from Takara Biochemicals (Tokyo, Japan). Acetonitrile was obtained from Merck KGaA (Darmstadt, Germany), and reagents for protein sequencing were from Applied Biosystems (Foster City, CA). Chromatography columns were obtained as follows: μRPC C2/C18 (10 μm, 120 Å, 2.1 × 100 mm) and HiLoad Superdex 30 gel filtration (1.6 × 60 cm), Amersham Biosciences AB (Uppsala, Sweden); RP-Jupiter C18 (5 μm, 300 Å, 1 × 150 mm), Phenomenex (Torrance, CA); UNO S6 cation exchange, Bio-Rad; and Discovery® BIO wide pore C5 (5 μm, 300 Å, 10 × 250 or 4.6 × 150 mm), Sigma. An RNeasy® RNA isolation mini kit; a one-step RT-PCR kit; QIAquick® PCR purification, gel extraction, and plasmid isolation miniprep kits; a PCR cloning kit; and a HotStartTaq polymerase kit were purchased from Qiagen Inc. An ABI PRISM BigDye terminator cycle sequencing ready reaction kit was purchased from Applied Biosystems. Gene-specific primers were custom-synthesized by 1st BASE (Singapore). 1 Kb Plus DNA Ladder™ was purchased from Invitrogen. EcoRI restriction endonuclease was obtained from New England Biolabs (Beverly, MA). LB-broth and agar were purchased from Qbiogene (Irvine, CA). Water was purified with a Milli-Q system (Millipore Corp., Billerica, MA). For protein synthesis, protected amino acid derivatives, resins, dicyclohexylcarbodiimide, and *N*-hydroxybenzotriazole were from Novabiochem (Meudon, France). Piperidine, *N*-methylpyrrolidone, dichloromethane, methanol, trifluoroacetic acid, and *tert*-butyl methyloxide were from SDS (Peypin, France). Tris(2-carboxyethyl)phosphine hydrochloride was from Pierce.

Snake Venoms—*B. dendrophila* venom was extracted as described previously (23) from snakes originating from Sulawesi, Indonesia. *Bungarus multicinctus* venom was obtained from Venom Supplies Pty. Ltd. (Tanunda, South Australia, Australia), and α-bungarotoxin was purified using a standard method (24).

Animals—Swiss-Webster albino mice (32 ± 2 g of body weight) were purchased from the Laboratory Animals Center of the National University of Singapore (Sembawang, Singapore) and kept in the Department of Pharmacology animal holding unit. Paper pellet bedding and food was purchased from Glen Forrest Stockfeeders (Glen Forrest, Western Australia, Australia). Food and water were available *ad libitum.* The animals were housed five per cage in a light-controlled room (12-h light/dark cycles) at 23 °C and 60% relative humidity.

6–10-day-old domestic chicks (*Gallus domesticus*) were purchased from an agricultural farm in Singapore and delivered on the day of experimentation. Experimental animals were killed by exposure to 100% CO_2.

Protein Purification—Previously, we had performed liquid chromatography/mass spectrometry crude venom profiling of *B. dendrophila* venom (25) to identify venom complexity and to predict the composition of venom proteins. A major protein component was purified from the venom using a two-step process involving cation exchange chromatography and reversed-phase high pressure liquid chromatography (RP-HPLC). Crude venom was applied to a UNO S6 cation exchange column attached to an ΔKTA purifier system (Amersham Biosciences AB) and separated into fractions with a linear gradient of 0–50% solvent B over 50 min (solvent A = 50 mM Tris-HCl (pH 7.5); solvent B = 1 M NaCl in 50 mM Tris-HCl (pH 7.5)). The pooled fractions containing the protein of interest were applied to an RP-Jupiter C18 HPLC column using the same chromatography system and eluted with a linear gradient of 30–40% solvent B over 80 min (solvent A = 0.1% trifluoroacetic acid in H_2O and solvent B = 80% acetonitrile and 0.1% trifluoroacetic acid in H_2O). Elution was monitored at 215 and 280 nm. To assess potential protein oligomerization, the purified lyophilized protein was diluted to 4 mg/ml in H_2O, incubated for 30 min at room temperature, and applied to a Superdex 30 gel filtration column attached to an ΔKTA purifier system. Protein was eluted with 50 mM Tris-HCl (pH 7.4) at a flow rate of 1 ml/min. Elution was monitored at 215 and 280 nm.

Mass Analysis—A Sciex API300 LC/MS/MS mass spectrometer (PerkinElmer Life Sciences, Thornton, Canada) was used to determine the precise masses and purity of the native protein as well as the generated peptides. Ion spray, orifice, and ring voltages were set at 4600, 50, and 350 V, respectively. Nitrogen was used as a curtain gas at a flow rate of 0.6 μl/min and as a nebulizer gas at a pressure setting of 100 p.s.i. The mass was determined by direct injection at a flow rate of 50 μl/min using a Shimadzu LC-10AD liquid chromatography pump as the solvent delivery system (50% acetonitrile and 0.1% formic acid in

H_2O). BioMultiView software was used to analyze the mass spectra.

Unblocking and Sequencing of the N Terminus—*Pfu* pyroglutamate aminopeptidase digestion was performed to remove the pyroglutamic acid residue that was blocking the N terminus of the protein. Enzymatic digestion was carried out in 50 mM sodium phosphate (pH 7.0) containing 10 mM dithiothreitol and 1 mM EDTA at a ratio of 2 milliunits of enzyme to 1 nmol of protein. The reaction was incubated for 10 h at 50 °C, followed by N-terminal sequencing by automated Edman degradation using an ABI Procise 494 pulsed-liquid phase protein sequencer (PerkinElmer Life Sciences) with an on-line 785A phenylthiohydantoin-derivative analyzer.

Peptide Generation and Protein Sequencing—Lyophilized protein (500 μg) was dissolved in 500 μl of 0.13 M Tris-HCl, 1 mM EDTA, and 6 M guanidine HCl (pH 8.5) and reduced with 10 μl of β-mercaptoethanol. This mixture was incubated at 37 °C for 2 h under N_2. Subsequently, 100 μl of alkylating reagent (4-vinylpyridine) was added, and the mixture was incubated for another 2 h under N_2 at room temperature in the dark. The alkylated toxin mixture was immediately loaded onto a μRPC C2/C18 column attached to a Smart workstation (Amersham Biosciences AB). The column was washed for 30 min with solvent A (0.1% trifluoroacetic acid in H_2O), followed by protein elution with a linear gradient of 0–50% solvent B (80% acetonitrile and 0.1% trifluoroacetic acid in H_2O). Lyophilized pyridylethylated protein was then subjected to enzymatic digestion with Lys-C endopeptidase or trypsin. Protein (250 μg) was dissolved in 250 μl of enzymatic digestion buffer (50 mM Tris-HCl, 4 M urea, and 5 mM EDTA (pH 7.5)), and proteases were added at a ratio of 1:50 (w/w). Cleavages were performed at 37 °C for 16 h. The peptides generated were separated on a μRPC C2/C18 column attached to the same chromatography system using a linear gradient of 15–40% solvent B over 1 h (solvent A = 0.1% trifluoroacetic acid in H_2O and solvent B = 80% acetonitrile and 0.1% trifluoroacetic acid in H_2O). The flow rate was 200 μl/min. Eluted peptides were monitored at 215, 254, and 280 nm. The amino acid sequences of the peptides were obtained by automated Edman degradation using an ABI Procise sequencer.

Total RNA Isolation—5 days after milking, the *B. dendrophila* specimen was killed by an overdose of CO_2. The pair of venom glands was dissected and stored in RNA*later* at −80 °C until used. Total RNA extraction was performed using a rotor homogenizer and an RNeasy mini kit. The amount of RNA was calculated according to the absorbance of the sample at 260 nm.

Reverse Transcription (RT)-PCR—Based on the available amino acid sequence of the protein, the following degenerate primers were designed to obtain partial cDNA sequence: RT-forward, 5′-GCICCIGTRCARCAYTTIAC-3′; and RT-reverse, 5′-TGYTTIGCIGTIGGMCACAT-3′. One-step RT-PCR was carried out using 100 ng of total RNA under the following conditions: RT at 50 °C for 30 min, followed by activation of HotStartTaq polymerase at 95 °C for 15 min and 30 cycles of three-step PCR (94 °C for 1 min, 50 °C for 1 min, and 72 °C for 1 min) and a final extension at 72 °C for 10 min. PCR products were subjected to 1% agarose gel electrophoresis and visualized by ethidium bromide staining.

Cloning and Sequencing of RT-PCR Products—Amplification products were purified using a PCR purification kit, ligated with the pDrive vector, and transformed by a heat shock method into competent *Escherichia coli* DH5α cells. Selection of the transformants (blue/white colony screening) was performed on LB-agar plates containing 100 μg/ml ampicillin and supplemented with X-gal (isopropyl β-D-thiogalactopyranoside and 5-bromo-4-chloro-3-indolyl-β-D-galactopyranoside). The sizes of the inserts were estimated by EcoRI digestion, followed by 1% agarose gel electrophoresis and ethidium bromide visualization. All sequencing reactions were carried out with an ABI PRISM 3100 automated DNA sequencer using a BigDye terminator cycle sequencing ready reaction kit according to the manufacturer's instructions. All clones were sequenced in both directions using T7 and SP6 sequencing primers.

Sequence Analysis—Sequence analysis was carried out using the BLAST program at the NCBI Database (www.ncbi.nlm.nih.gov) and ExPASy proteomics tools (www.expasy.ch). Sequence alignments were carried out using the ClustalW program (www.ebi.ac.uk) or DNAMAN Version 4.15 (Lynnon Corp.).

Chemical Synthesis—Chemical synthesis and assembly of protein were performed with an Applied Biosystems 431 peptide synthesizer using a modified version of the Applied Biosystems standard 0.1 mmol small-scale program (26) with *N*-hydroxybenzotriazole as the coupling reagent and *N*-methylpyrrolidone as the solvent. Fmoc-protected amino acids were used with the following side chain protections: *t*-butyl ester (Glu and Asp), *t*-butyl ether (Ser, Thr, and Tyr), *t*-butylcarbonyl (Lys), trityl (Cys, His, Asn, and Gln), 2,2,5,7,8-pentamethylchromane-6-sulfonyl (Arg), and *t*-butyloxycarbonyl (Trp). The toxin was assembled on Fmoc-Asp-*t*-butoxy-Wang resin (loading, 0.55 mmol/g) (27). Synthesis was performed using the improved software armed with UV deprotection step monitoring, which, in the case of deprotection failure, automatically extends the deprotection and coupling time for the particular amino acid (28). After each coupling, the resin was acetylated with a mixture of 5% acetic anhydride and 6% 2,4,6-collidine in dimethylformamide. At the end of the synthesis, the peptide resin was treated with a mixture of trifluoroacetic acid (90%), triisopropylsilane (5%), and distilled water (5%) to cleave the peptide from the resin and to remove the protecting groups from amino acid side chains. After 2 h of incubation at room temperature with constant mixing, the crude material was filtered and precipitated in cold *tert*-butyl methyloxide. Precipitates were washed three times with *tert*-butyl methyloxide, followed by centrifugation at 1700 × *g* and resuspension in 10% acetic acid. Lyophilized crude synthetic toxin was then reduced with a molar excess of tris(2-carboxyethyl)phosphine hydrochloride for at least 30 min (to reduce incorrectly formed disulfide bonds) and purified by RP-HPLC using a Discovery® BIO wide pore C5 column (10 × 250 mm) with a gradient of 40–60% of solvent B over 40 min (solvent A = 0.1% trifluoroacetic acid in H_2O and solvent B = 60% acetonitrile and 0.1% trifluoroacetic acid in H_2O). The flow rate was 3 ml/min, and elution was followed at 215 and 280 nm.

Purification and Refolding of the Synthetic Toxin—The reduced synthetic peptide was dissolved in 200 μl of distilled

water to evaluate protein concentration based on absorbance at 278 nm. It was then diluted with refolding buffer (0.1 M Tris-HCl (pH 7.8) and 0.5 M guanidium chloride, GSH, and GSSH at a molar ratio of 10:1) to a concentration of 0.05 mg/ml and incubated for 2–4 days in 4 °C. The mixture was acidified with 20% trifluoroacetic acid and purified on a Discovery® BIO wide pore C5 column with a gradient of 30–50% solvent B over 40 min (solvent A = 0.1% trifluoroacetic acid in H_2O and solvent B = 60% acetonitrile and 0.1% trifluoroacetic acid in H_2O). The flow rate was 3 ml/min, the elution was followed at 215 and 280 nm. The synthetic and native toxins were compared by co-elution profiles and circular dichroism spectra.

In Vivo Toxicity Test—The native protein was injected intraperitoneally into male Swiss-Webster mice (19 ± 2 g) at 0.1, 1, 10, and 20 mg/kg ($n = 2$). All doses were made up to a volume of 200 μl in saline. The same volume of normal saline was injected intraperitoneally into control animals. Mice were observed for 6–8 h and killed after 24 h for autopsy. Mice (19 ± 2 g) were injected intracerebroventricularly with the protein at 0.1, 1, and 10 mg/kg in 5 μl of saline ($n = 2$ per dose) or with 5 μl of control saline ($n = 2$) using a fine capillary Hamilton microsyringe. Animals were killed for autopsy after 5 h of observation.

Chick Biventer Cervicis Muscle (CBCM) Preparations—Pairs of CBCMs were isolated from 6–10-day-old chicks and mounted in an 8-ml organ bath (29) containing Krebs solution continuously aerated with 5% CO_2 in O_2. The temperature of the organ bath was maintained at 35 °C. The resting tension of the isolated tissue was adjusted to ~1 g. Electrical field stimulation was carried out through platinum ring electrodes using an S88 stimulator (Grass Instruments, Quincey, MA). The data were transferred via a Model FT03 force displacement transducer (Grass Instruments) and recorded using a PowerLab 6 system (ADInstruments, Bella Vista, New South Wales, Australia). Maximal twitch responses of the muscle were elicited indirectly via stimulation of the motor nerve by applying an electrical field of 7–10-V potential difference at a frequency of 0.2 Hz in supramaximal rectangular pulses of 0.1-ms duration. The preparation was equilibrated for 30–50 min before the beginning of an experiment, with changes of Krebs solution at 10-min intervals. To ensure selective stimulation of the motor nerve, *d*-tubocurarine (10 μM) was added, with subsequent abolition of twitches, which were then re-established after a thorough wash. At appropriate intervals, submaximal control contractures to exogenously applied 300 μM acetylcholine, 8 μM carbachol, or 30 mM KCl were obtained in the absence of an electrical field. The contact times for these agonistic drugs were 30, 90, and 60 s, respectively, followed by a wash with ~100 ml of fresh Krebs solution. The electrical stimulation was then recommenced; and after stabilization of twitch height, the effects of various concentrations of denmotoxin (0.1–100 μg/ml, 11.8 nM to 11.8 μM; $n = 5$), α-bungarotoxin (0.1 nM to 0.5 μM; $n = 3$), or vehicle were investigated. Neuromuscular blockage is expressed as a percentage of the original twitch height in the absence of toxin. Dose-response curves representing the percent blockage after 30 min of CBCM exposure to the respective toxins were plotted. Each preparation was exposed to only one dose of toxin, and both muscles from the same specimen were used to test two different doses. The reversibility of the inhibitory effect of the toxin on twitches was assessed by the replacement of Krebs solution in the organ bath at 10-min intervals combined with a slow drip wash over 180 min. The effect of neostigmine (10 μM) on the reversal of neuromuscular blockage was also examined.

Mouse Hemidiaphragm Muscle (MHD) Preparations—MHD with the associated phrenic nerve was isolated as described by Bulbring (30) and mounted in a 5.5-ml organ bath. Indirect stimulation was performed at a frequency of 0.2 Hz in rectangular pulses of 0.2-ms duration at a supramaximal voltage of 7–10 V. α-Bungarotoxin (10, 50, and 100 nM; $n = 3$) was used as a positive control. Partial dose-response curves for denmotoxin (117.5 nM, 1.175 μM, and 11.75 μM ($n = 3$) and 2.35 and 5.88 μM ($n = 1$)) were determined. In control experiments, the effect of uninterrupted nerve stimulation of MHD was assessed. Also, the recovery of twitches was assessed by washing with Krebs solution overflow, followed by slow drip wash. To eliminate batch-to-batch variations of the protein during the experiments, all CBCM and MHD experiments were performed using same protein stock solution. Data are expressed as the means ± S.E. Data were analyzed and fitted using Fig.P Version 2.98 (Fig.P Software Corp., Durham, NC).

Crystallization—Lyophilized protein was resuspended in 50 mM sodium acetate (pH 5.5) containing 0.02% sodium azide, washed four times to remove salts, and reconcentrated to 10 mg/ml by ultrafiltration with an Amicon 5-kDa cutoff filter (Millipore Corp.). Crystallization experiments were carried out using the sitting drop vapor diffusion method at 291 K (18 °C). In initial crystallization experiments, Hampton Research Crystal Screens 1 and 2 were used, and setups contained 1 μl of protein and 1 μl of reservoir solution. The final conditions were optimized by seeding to bypass spontaneous nucleation and hence to control the number of crystals and to improve their growth. Crystals for diffraction were kept in cryoprotectant solution containing 1.5 M $LiSO_4$ and 25 mM imidazole (pH 8.0) and flash-frozen in liquid ethane.

X-ray Diffraction Data Collection, Structure Determination, and Refinement—Crystal diffraction was performed on beam line ID-29 at the European Synchrotron Radiation Facility (Grenoble, France). The data were processed using the HKL package (31), and the structure was solved using the molecular replacement method. Different search models were tried out to find the proper rotation and translation solution. To choose the best model for the molecular replacement method, a FASTA search was conducted using the protein sequence against the Protein Data Bank. The closest match found was the crystal structure of neurotoxin-1 from *Naja naja oxiana* (PDB code 1NTN). Based on this molecule, the denmotoxin search model was built by residue replacement. Several other homology models were tried in a different resolution range, but no solution could be found. Finally, the proper solution was found using native data and a search model built based on irditoxin (PDB code 2H7Z) with partial deletions of loops regions. The programs MOLREP (32), Refmac (33), CNS (34), and PROCHECK (35) were used to solve, refine, and analyze the structure.

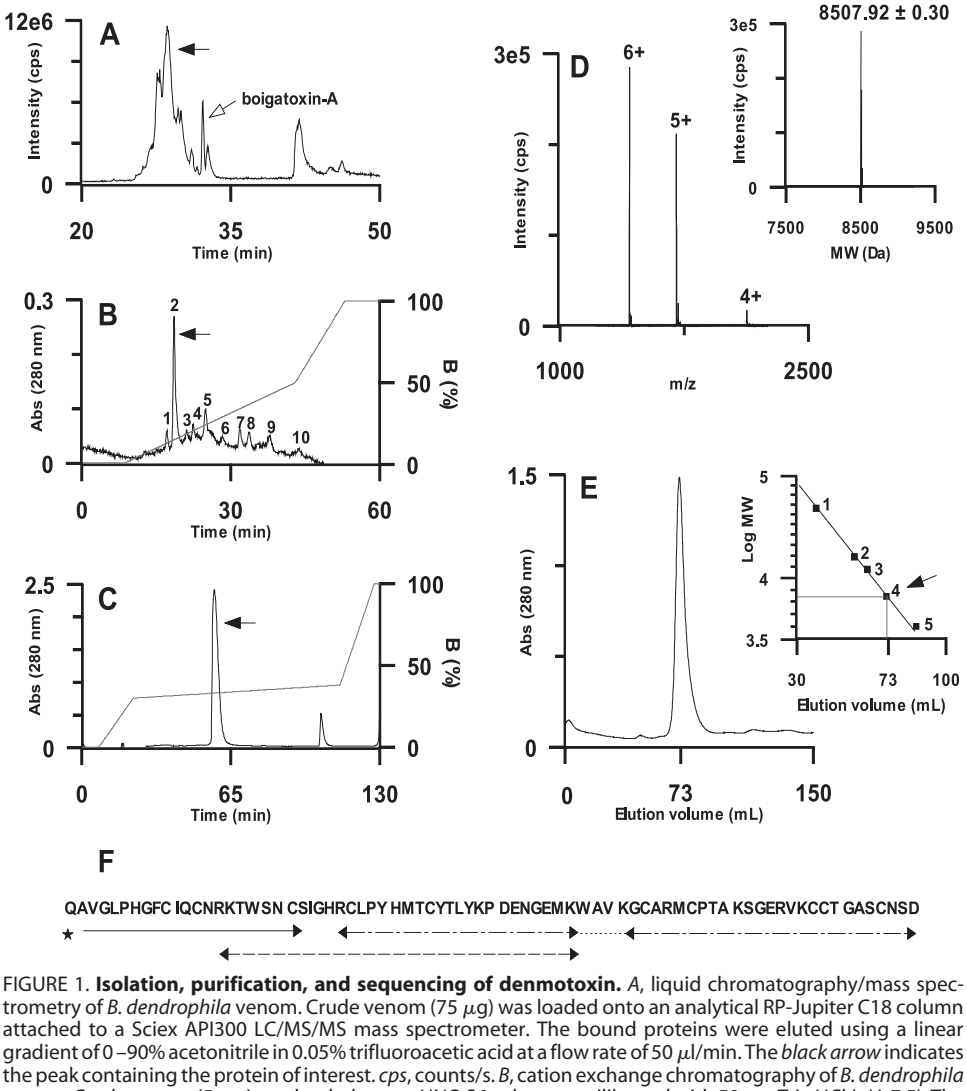

FIGURE 1. **Isolation, purification, and sequencing of denmotoxin.** *A*, liquid chromatography/mass spectrometry of *B. dendrophila* venom. Crude venom (75 μg) was loaded onto an analytical RP-Jupiter C18 column attached to a Sciex API300 LC/MS/MS mass spectrometer. The bound proteins were eluted using a linear gradient of 0–90% acetonitrile in 0.05% trifluoroacetic acid at a flow rate of 50 μl/min. The *black arrow* indicates the peak containing the protein of interest. *cps*, counts/s. *B*, cation exchange chromatography of *B. dendrophila* venom. Crude venom (5 mg) was loaded onto a UNO S6 column equilibrated with 50 mM Tris-HCl (pH. 7.5). The bound proteins were eluted with a linear gradient of solvent B (1 M NaCl in 50 mM Tris-HCl (pH. 7.5)). Fraction 2 (indicated by the *arrow*) contained the protein of interest. *Abs*, absorbance. *C*, RP-HPLC of fraction 2 on a Jupiter C18 column using a shallow gradient (30–40% over 80 min) of solvent B (80% acetonitrile in 0.1% trifluoroacetic acid). The peak (*arrow*) contained a single homogeneous protein that we named denmotoxin. *D*, ESI/MS of denmotoxin. The spectrum shows a series of multiply charged ions corresponding to a homogeneous protein with a molecular mass of 8507.92 ± 30 Da (*inset*). *E*, confirmation by gel filtration on a Superdex 30 column using 50 mM Tris-HCl (pH 7.4) as eluent that denmotoxin is a monomer. *Inset*, the elution volumes of several proteins were plotted against their molecular masses to generate a standard curve: ovalbumin (45.9 kDa; *square 1*), ribonuclease (15.6 kDa; *square 2*), cytochrome *c* (12 kDa; *square 3*), aprotinin (7 kDa; *square 4*), and leupeptin (4 kDa; *square 5*). The molecular mass of denmotoxin was determined by its elution volume (indicated by the *arrow*). *F*, determination of the amino acid sequence of denmotoxin. The removal of pyroglutamic acid from the N terminus using pyroglutamate aminopeptidase is indicated by the *asterisk*. N-terminal sequencing of the unblocked pyridylethylated protein by Edman degradation is indicated by the *solid arrow*. The sequences of one Lys-C and two tryptic peptides are indicated by the *dashed* and *dashed-dotted arrows*, respectively. The sequence deduced from the cDNA sequence is indicated by the *thin dotted line*.

RESULTS

Identification and Purification of the Toxin—A liquid chromatography/mass spectrometry profile revealed that the most abundant proteins in the crude venom *of B. dendrophila* have molecular masses ~8–10 kDa (25). Among them, we have identified one major component with a mass of ~8508 Da (Fig. 1*A*). This protein was purified to homogeneity by consecutive cation exchange chromatography (Fig. 1*B*) and RP-HPLC (Fig. 1*C*). *B. dendrophila* venom was separated into 10 fractions on a UNO S6 column (Fig. 1*B*). Each peak was then subjected to RP-HPLC, and the individual fractions from RP-HPLC were assessed by electrospray ionization mass spectrometry (ESI/MS) (data not shown). Peak 2 from the cation exchange column (Fig. 1*B*) contained the protein of interest (Fig. 1*C*). The protein was found to be homogeneous, with a precise molecular mass of 8507.92 ± 0.30 Da as determined by ESI/MS (Fig. 1*D*). The purification yielded ~5 mg of toxin from 100 mg of crude venom. The protein was confirmed to be a monomer by gel filtration chromatography (Fig. 1*E*), as only one peak eluted at a retention time of 73 min, corresponding to a mass of ~8 kDa (monomeric). We named this protein denmotoxin for *B. dendrophila* monomeric toxin.

Determination and Analysis of the Amino Acid Sequence—The first attempt to obtain the N-terminal sequence of denmotoxin by Edman degradation failed, as the toxin was N-terminally blocked by pyroglutamic acid. Pyroglutamate aminopeptidase was used to remove the blocking group. N-terminal sequencing of the unblocked protein resulted in identification of the first 20 residues (Fig. 1*F*). Further sequence data were obtained by the generation and sequencing of peptides following digestion of the pyridylethylated protein with lysyl endopeptidase and trypsin (Fig. 1*F*). Peptides from respective digests were separated by RP-HPLC (data not shown) and subjected to automated Edman degradation. More than 90% of the sequence (except the WAVK fragment) was determined by protein sequencing (Fig. 1*F*). Based on the available amino acid sequence, degenerate primers were designed to fish out the missing fragment by RT-PCR and to determine the complete sequence of the toxin. Using this strategy, we were able to identify unequivocally all residues of denmotoxin (GenBank™ accession number DQ366293). The protein possesses 77 amino acid residues, including 10 cysteines (Fig. 2). The calculated mass of denmotoxin, with the observed pyroglutamation and five disulfide bridges, is 8507.8 Da, nearly identical to the observed molecular mass (8507.92 ± 0.30 Da) estimated by ESI/MS (Fig. 1*D*). The multiple sequence alignment, in particular, the arrangement of the cysteines (Fig. 2), indicates that denmotoxin belongs to the

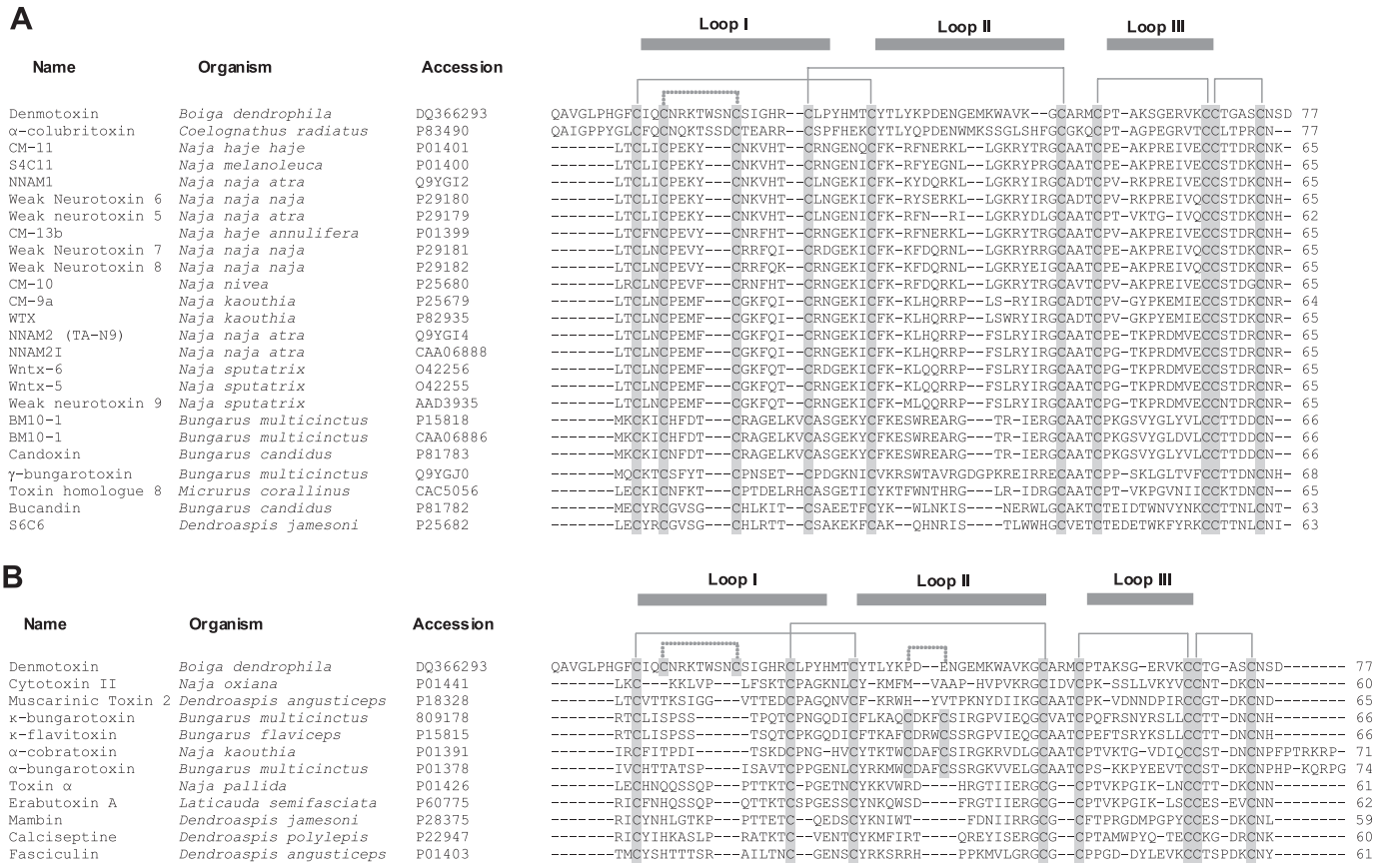

FIGURE 2. **Multiple sequence alignment of denmotoxin with non-conventional toxins (*A*) and three-finger toxins (*B*).** Toxin names, species, and Swiss-Prot accession numbers are shown. Cysteines are marked highlighted in *gray*. Disulfide bridges and loop regions are also shown.

class of non-conventional 3FTXs (3). Denmotoxin differs structurally from elapid 3FTXs in having seven additional residues at its N terminus, which is blocked by a pyroglutamic acid residue (Fig. 2). In this respect, it is similar to 3FTXs isolated from colubrid venoms such as α-colubritoxin (18) and boigatoxin-A (25). Denmotoxin shares ~50% identity with α-colubritoxin, but it shows <30% identity to elapid 3FTXs (Fig. 2) and only ~15–20% identity if the five disulfide bridges (which contribute significantly to the percentage of identity) are excluded.

Synthesis and Characterization of Synthetic Denmotoxin—The investigation of colubrid venom components is severely limited because of the tedious extraction procedure and low venom yields (23). Therefore, we chemically assembled denmotoxin by solid-phase peptide synthesis. The yield from peptide synthesis was ~30% based on deprotection monitoring at 301 nm. Reduced crude peptide was purified from contaminating side products by RP-HPLC (Fig. 3*A*). The major peak contained a homogeneous peptide with a molecular mass of 8517.38 ± 0.44 Da as assessed by ESI/MS (Fig. 3*B*), which precisely matched the calculated mass for the reduced form of denmotoxin (8517.8 Da). This reduced synthetic denmotoxin was subjected to glutathione-mediated oxidation, followed by acidification and RP-HPLC purification. The oxidized peptide eluted as a major component ~10 min earlier than the reduced form (data not shown); therefore, for greater purification, the gradient was modified (Fig. 3*C*). The oxidized synthetic denmotoxin was homogeneous, with a molecular mass of 8507.70 ± 0.22 Da (Fig. 3*D*), which exactly matched the mass of the native protein. Furthermore, the native and synthetic proteins were shown to be identical based on co-elution profiles by RP-HPLC (Fig. 3*E*) and CD spectroscopy analysis (data not shown). To compare the pharmacological action of the synthetic and native denmotoxin proteins, we tested both preparations in CBCM experiments. Our results indicate that they displayed identical physicochemical and pharmacological properties.

Species-specific Neuromuscular Blockage—Denmotoxin caused time- and concentration-dependent blockage of the twitch responses in indirectly stimulated CBCM preparations (Fig. 4). It also completely inhibited contractile responses of the exogenously applied nicotinic agonists (acetylcholine and carbachol) (Fig. 4*A*) but did not show any inhibition of 50 mM KCl (Fig. 4*A*) or direct twitches in the preparation (data not shown). Thus, denmotoxin acts as a postsynaptic neurotoxin. The neuromuscular blockage was virtually irreversible and sustained for up to 180 min without spontaneous reversal despite washing the organ bath with Krebs solution (Fig. 4*A*). The addition of neostigmine (10 μM) to tissues treated with 0.24 μM denmotoxin did not restore partially diminished nerve-induced twitches (data not shown). Similarly, α-bungarotoxin produced pseudo-irreversible blockage, which was not affected by washing or by neostigmine addition (data not shown). However, α-bungarotoxin was 10-fold more potent than denmotoxin (Fig. 4*C*).

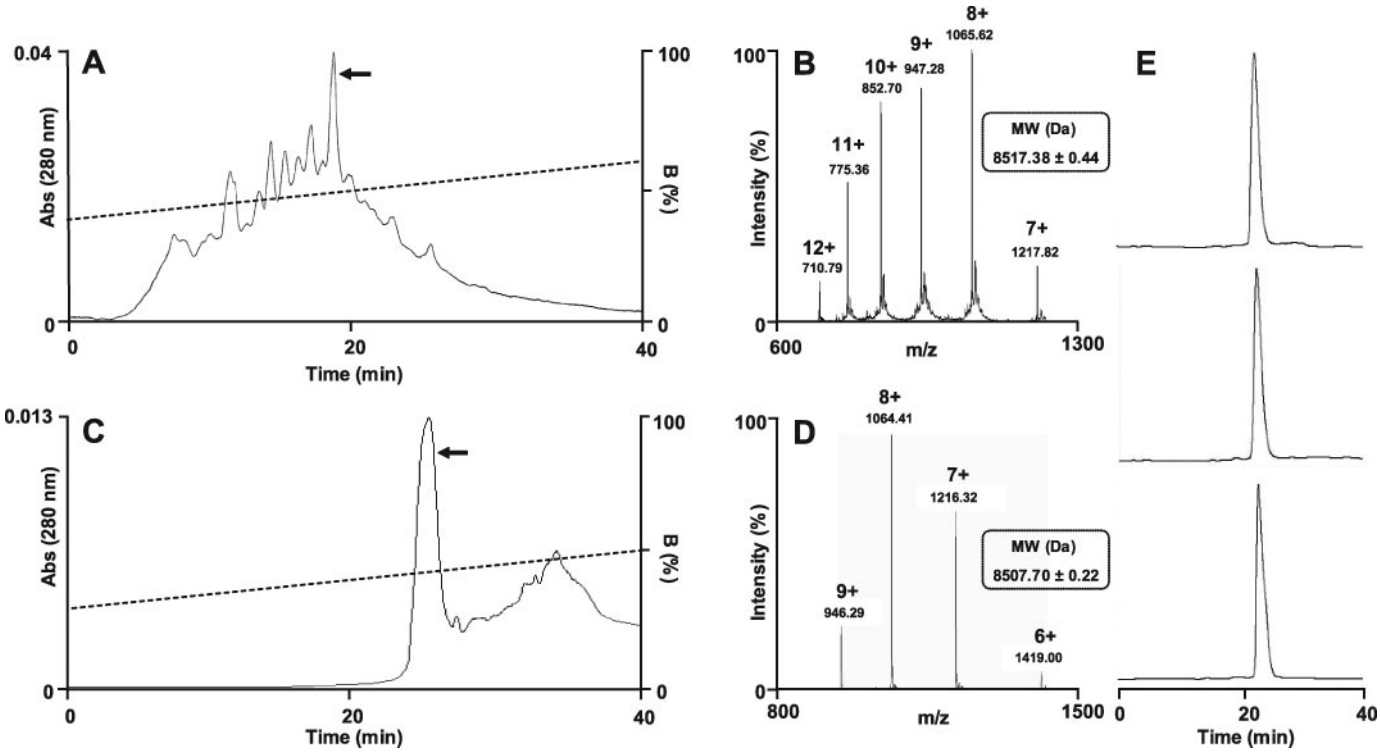

FIGURE 3. **Purification and characterization of synthetic denmotoxin.** *A*, RP-HPLC of reduced crude material on an analytical Discovery® BIO wide pore C5 column (4.6 × 150 mm) eluted with a gradient of 40–60% solvent B (solvent A = 0.1% trifluoroacetic acid in H_2O and solvent B = 60% acetonitrile and 0.1% trifluoroacetic acid in H_2O) over 40 min at a flow of 1 ml/min. The *arrow* indicates the peak corresponding to reduced synthetic denmotoxin. *Abs*, absorbance. *B*, ESI/MS of purified synthetic denmotoxin with 10 reduced cysteine residues. The spectrum shows a series of multiply charged ions corresponding to the correct molecular mass of 8517.38 ± 0.44 Da. *C*, RP-HPLC of refolded synthetic denmotoxin purified on a Discovery® BIO wide pore C5 column (5 μm, 300 Å, 0.1 × 25 cm) with a gradient of 30–50% solvent B over 40 min (solvent A = 0.1% trifluoroacetic acid in H_2O and solvent B = 60% acetonitrile and 0.1% trifluoroacetic acid in H_2O). The *arrow* indicates the peak corresponding to properly refolded synthetic denmotoxin. *D*, ESI/MS of refolded synthetic denmotoxin. The spectrum shows a series of multiply charged ions corresponding to the correct molecular mass of 8507.70 ± 0.22 Da. *E*, co-elution of native and synthetic denmotoxin proteins. RP-HPLC was performed on an analytical Discovery® BIO wide pore C5 (4.6 × 150 mm) column with a gradient of 30–50% solvent B over 40 min (solvent A = 0.1% trifluoroacetic acid in H_2O and solvent B = 60% acetonitrile and 0.1% trifluoroacetic acid in H_2O). The flow rate was 1 ml/min. Profiles of the native toxin (*upper trace*), the synthetic toxin (*middle trace*), and an equimolar mixture of the native and synthetic toxins (*lower trace*) are shown; note that all chromatograms show the same elution time.

In contrast, denmotoxin showed a very weak effect on neuromuscular transmission in MHD preparations. The blockage produced by denmotoxin in MHD was up to 100-fold smaller than that produced in CBCM, and denmotoxin was not able to produce complete blockage of indirectly stimulated twitches up to 11.76 μM (Fig. 4*C*). Moreover, unlike irreversible denmotoxin-induced blockage in CBCM, that in MHD was rapidly reversed by washing (Fig. 4*B*). In contrast, the positive control (α-bungarotoxin) used in MHD experiments virtually irreversibly blocked with a similar dose-response curve as in CBCM experiments (Fig. 4*C*). Thus, denmotoxin induces partial and reversible blockage of neurotransmission in MHD. In agreement with this finding, we observed no paralysis or other biological effects in mice after intraperitoneal or intracerebroventricular injection of the toxin at up to 20 and 10 mg/kg, respectively. Taken together, these results indicate a clear species-dependent toxicity and susceptibility of chick muscle nAChR to denmotoxin.

Three-dimensional Structure—We determined the three-dimensional structure of denmotoxin, a unique 3FTX with an unusually long N-terminal segment, by crystallization and x-ray diffraction methods. The most suitable crystals were obtained in a solution containing 1.2 M $NaKPO_4$ (NaH_2PO_4 + K_2HPO_4) at pH 7. They belong to monoclinic space group C2, with two molecules of denmotoxin per asymmetric unit. The crystal diffracted to 1.7 Å on a synchrotron beam line, and the structure of denmotoxin was solved using the molecular replacement method. The model was refined to 1.9 Å, and the PROCHECK program confirmed the standard stereochemistry. The statistics for data collection and refinement are shown in Table 1. Coordinates of the structure have been deposited in the Protein Data Bank (code 2H5F). The electron density maps were excellent for the whole molecule except for the three first residues at the N terminus and the tip of the central loop, suggesting high flexibility in these regions. 284 water molecules and four phosphate, two potassium, and two sodium ions from the mother liquor ($NaKPO_4$) were also identified in these electron density maps. Two phosphate ions are located near Arg^{55} of the respective molecules, whereas two others (near Arg^{26}) seem to stabilize intermolecular interactions and to contribute to crystallographic dimer formation. The structure of denmotoxin is similar to those of other 3FTXs (Fig. 5*B*). Erabutoxin-b (*Laticauda semifasciata*), bucandin (*Bungarus candidus*), toxin-b (*Ophiophagus hannah*), and toxin-γ (*Naja nigricollis*) show the closest match as shown by the Dali search algorithm (36). Denmotoxin consists of three polypeptide loops, with four disulfide bridges holding the molecule at the central core and a fifth disulfide bridge located at the tip of the first loop (Fig. 5*A*),

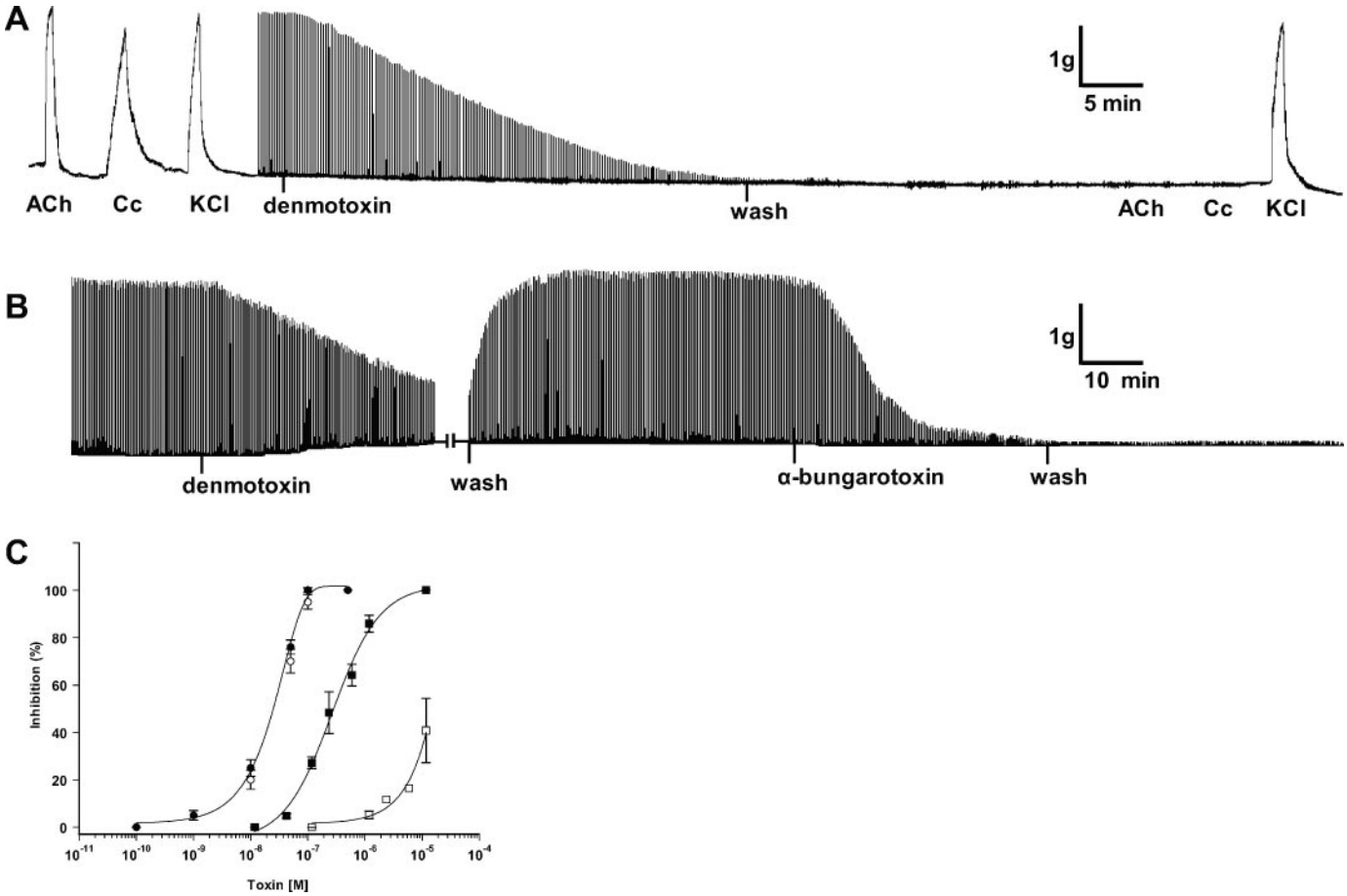

FIGURE 4. **Neuromuscular blockage produced by denmotoxin.** *A*, segment of a trace showing the irreversible blockage of nerve-induced twitches produced by denmotoxin (10 μg/ml, 1.176 μM) in CBCM. Contractions produced by exogenous acetylcholine (*Ach*; 300 μM), carbachol (*Cc*; 8 μM), and KCl (30 mM) before and after treatment with toxin are also shown. *B*, segment of a trace showing the readily reversible blockage of nerve-induced twitches produced by denmotoxin (100 μg/ml, 11.76 μM) in MHD. In contrast, α-bungarotoxin (0.1 μM) produced irreversible blockage. *C*, dose-response curves for the neuromuscular blockage produced by α-bungarotoxin (*circles*) and denmotoxin (*squares*) in the CBCM (*closed symbols*) and MHD (*open symbols*) preparations after 30 min of exposure to the respective toxins.

as is also found in elapid non-conventional toxins (3). The major element of the secondary structure is a triple-stranded antiparallel β-sheet consisting of two strands from the second loop and one strand from the third loop. Despite being a representative of the 3FTX family, denmotoxin displays unique features such as the twisted tip of the central loop, which originates from the kink of Pro^{40} (Fig. 5, *A* and *B*). The unusually long N-terminal segment of seven residues is clearly unstructured and probably flipping above the core of the molecule (Fig. 5, *A* and *B*), the first three N-terminal residues not even being seen in the electron density map. The surface charge density of denmotoxin is relatively uneven, and the electrostatic potential of the tip of the central loop is negative, unlike other neurotoxins of the 3FTX family (Fig. 5*C*). The crystal structure of denmotoxin is the first high resolution structure of a colubrid 3FTX, and it provides a platform for further investigations to decipher the basis of denmotoxin interactions with the target receptor.

DISCUSSION

Snake venoms are a rich source of pharmacologically active proteins and polypeptides. A number of toxins have provided excellent research tools used to decipher the molecular details of physiological processes, and several have led to the development of novel therapeutic agents (37, 38). Among snake venoms, colubrid venoms are the least studied because of the lack of commercial sources, the difficulty in extraction procedures, and the low yield of venoms (22); thus, the chemistry of the venoms from this large group of snakes is poorly understood. As colubrids have a distinct evolutionary lineage, they are expected to provide interesting new groups of protein toxins. Indeed, in this study, we isolated and characterized a novel colubrid toxin (denmotoxin) from *B. dendrophila* venom. The mature protein has 77 amino acid residues, including 10 cysteines, and belongs to the non-conventional class of the 3FTX family. However, it shows low sequence identity to other 3FTXs and has an extended N-terminal segment that appears to be unique to colubrid venoms. Pharmacological studies revealed that denmotoxin is a taxon-specific postsynaptic neurotoxin. The high resolution crystal structure shows that it structurally resembles other elapid 3FTXs, but it also possesses the unusually long N-terminal flipping above the core of molecule and a twisted central loop negatively charged at its tip. This study has provided the first description of the pharmacological and structural properties of a colubrid toxin.

TABLE 1
Crystallographic data and refinement statistics
r.m.s.d., root mean square deviation.

Data collection	
Resolution range (Å)	52 to 1.7
Wavelength (Å)	1.006768
Observed reflections >1	50,240
Unique reflections	16,784
Completeness (%)	93.5
Overall ($I/\sigma I$)	8.5
R_{sym} (%)[a]	10.3
Space group	C2
Cell parameters (Å)	98.91, 34.04, 54.38, 90, 90 (118.36°)
Refinement	
Resolution range (Å)	47 to 1.9
R_{work} (no. reflections)[b]	20.19 (11,487)
R_{free} (no. reflections)[c]	23.84 (584)
r.m.s.d. bond lengths (Å)	0.032
r.m.s.d. bond angles	2.088°
Average *B*-factors (Å^2)	
Main chain	17.05
Side chains	20.83
Ramachandran plot	
Most favored regions (%)	83.1
Additional allowed regions (%)	15.3
Generously allowed regions (%)	1.6
Disallowed regions (%)	0

[a] $R_{sym} = \Sigma|I_i - \langle I\rangle|/\Sigma|I_i|$, where I_i is the intensity of the *i*th measurement and $\langle I\rangle$ is the mean intensity for that reflection.
[b] $R_{work} = \Sigma|F_o - F_c|/\Sigma|F_o|$, where F_c and F_o are the calculated and observed structure factor amplitudes, respectively.
[c] R_{free} is as for R_{work}, but for 5% of the total reflections chosen at random and omitted from refinement.

In an attempt to obtain denmotoxin in larger quantities, we synthesized it by solid-phase peptide synthesis using Fmoc chemistry. The synthesis of denmotoxin without using chemical ligation was challenging, as the protein is a 77-amino acid residue long β-sheeted polypeptide that is rich in disulfide bridges and therefore prone to aggregation and incorrect disulfide formation. To enhance the assembly, UV monitoring of deprotection and automatic extension of the deprotection time to 20 min and of the coupling time to 30 min were used when the deprotection was not sufficient after two successive 3-min deprotections. Using this method, the overall yield of synthesis was ~30%, which is much higher than often obtained with peptides of this length. Peptide synthesis allowed us to obtain considerable quantities of the toxin without resorting to traditional purification methods. It should be emphasized that the oxidized synthetic peptide has all the biochemical characteristics of the natural toxin and was virtually indistinguishable from the native toxin in organ bath experiments. These results ruled out the possibility that the activity of native denmotoxin may be due to potential contaminants from the crude venom, as was shown in the case of κ-bungarotoxin containing a minor impurity of potent α-bungarotoxin (39). In addition, an Fmoc-based chemical approach might be useful for future mutagenesis studies of denmotoxin.

Venoms from snakes of the genus *Boiga* exhibit postsynaptic neurotoxicity. For example, *Boiga blandingi* venom irreversibly inhibits motor end plate potential in frog nerve-muscle preparations (40); *Boiga irregularis* venom shows competitive binding with cobrotoxin to nAChRs in an enzyme-linked immunoassay (41); and partially purified components of *B. dendrophila* venom (~11 and 12 kDa) bind to *Torpedo marmorata* mAChRs (42). Recently, *B. dendrophila* venom (43, 44) and a toxin isolated from this venom, boigatoxin-A (Fig. 1*A*), have been shown to irreversibly block twitches in CBCM preparations. Boigatoxin-A (45) has a molecular mass of 8769 Da, and its N-terminal 47 residues show 78% identity to denmotoxin. Similar to boigatoxin-A, denmotoxin exhibits a postsynaptic neurotoxic effect in CBCM. Denmotoxin inhibited the indirect twitches and exogenous agonist responses, indicating its postsynaptic effects (Fig. 4). However, it exhibited neurotoxic effects differently in MHD experiments, being ~100-fold weaker and readily reversibly blocking the indirectly stimulated twitches, a finding that explains why denmotoxin neither paralyzes nor shows any other effects in mice after intraperitoneal injection even at 20 mg/kg. These data strongly suggest that denmotoxin is able to discriminate between the peripheral nAChRs from two species. Boigatoxin-A was tested only on chick (but not mice) neuromuscular junctions; hence, it is not clear whether it would also exhibit similar species specificity. Species-specific neurotoxicity is known for colubrid venoms. For example, the neurotoxicity of *Philodryas patagoniensis* venom (46, 47) is more specific to pigeons than to guinea pigs, rabbits, and frogs. Also, both the crude venom and partially purified venom components of *Philodryas olfersii* show postsynaptic neurotoxicity in CBCM preparations, whereas MHD preparations are unaffected (48). Recently, it was also demonstrated that the venom of *B. irregularis* displays taxon-specific toxicity (49), and denmotoxin is the first well characterized venom component that shows species-specific effects. It is interesting that the *B. dendrophila* snake preys primarily on birds (21). As there is a correlation between toxin specificity and a snake's diet (49), the major components in *B. dendrophila* venom have probably evolved to target birds. Denmotoxin may be one such toxin targeted to affect birds. Thus, care must be taken when studying the toxicity of such venoms, as LD_{50} studies conducted using mouse models only may not truly reflect the toxic potency of the venom components (22).

Denmotoxin shares <30% sequence identity with other 3FTXs (except α-colubritoxin), but it retains the residues involved in maintaining the three-finger fold. Much of this sequence identity is due to conserved disulfide bridges and several structurally important residues. Denmotoxin possesses all four conserved disulfide bridges located in the core region, the reduction of which has been shown to disturb the overall conformation and to result in total loss of function (50). In addition, denmotoxin has most of the invariant residues that are important for proper folding and the three-dimensional structure. Tyr^{25} (all numbering is according to erabutoxin-a) has been shown to be a highly conserved and structurally important residue (51, 52). Antil *et al.* (53) have shown that mutation of its equivalent in α-cobratoxin (Y21A) prevents proper folding of the protein. Moreover, Tyr^{21} was shown to stabilize the antiparallel β-sheet structure (54). Denmotoxin also possesses Tyr^{35} with the side chain oriented exactly in the same way, although, in most non-conventional toxins, this tyrosine is replaced by a homologous Phe^{25}. Another residue important for maintaining spatial conformation is Gly^{40}, placed opposite Tyr^{25} to accommodate the bulky side chain. The equivalent Gly is present as Gly^{52} in denmotoxin. Also, Pro^{44} has been shown to be structurally important (51), and it is represented by Pro^{58} in denmo-

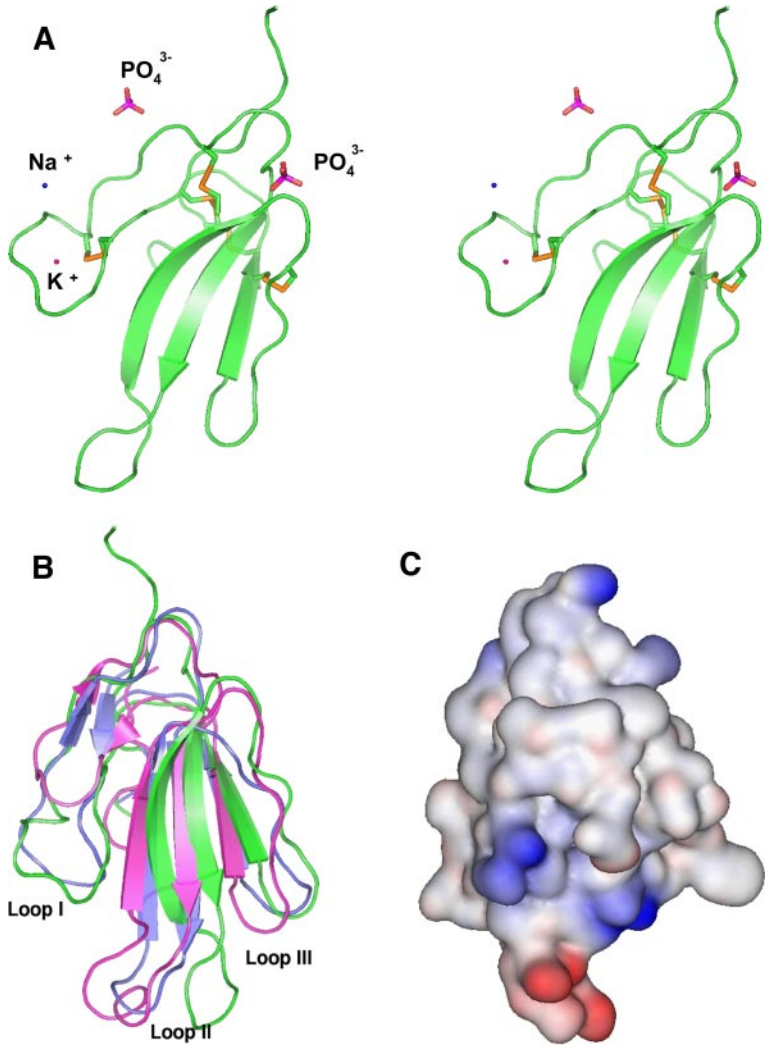

FIGURE 5. **Crystal structure of denmotoxin.** *A*, stereo view of the overall structure of denmotoxin. Cysteine bonds are shown in *yellow*. The two phosphate ions and the sodium and potassium ions are shown. *B*, superimposition of denmotoxin (*green*) with α-cobratoxin (PDB code 2CTX; *pink*) and erabutoxin-b (PDB code 3EBX; *violet*). *C*, surface plot of denmotoxin showing electrostatic potential and the negative tip of the central loop (*red*).

toxin. The presence of these structurally important residues in denmotoxin results in the retention of the characteristic three-finger fold, as is apparent from the crystal structure (Fig. 5*B*).

The functionally important residues involved in receptor binding in short- and long-chain neurotoxins have been studied in detail (55–58). Moreover, the recently determined crystal structure of α-cobratoxin complexed with acetylcholine-binding protein (AChBP) illustrates the critical residues involved in toxin-receptor interactions (59). Erabutoxin-a and α-cobratoxin interact with *Torpedo* $\alpha_1\beta\gamma\delta$-nAChRs using a common core of residues: Lys^{27}/Lys^{23}, Trp^{29}/Trp^{25}, Asp^{31}/Asp^{27}, Phe^{32}/Phe^{29}, Arg^{33}/Arg^{33}, and Lys^{47}/Lys^{49}. The first five of the these residues are replaced by unconserved residues in denmotoxin: Leu^{37}, Lys^{39}, Gly^{44}, Glu^{42}, and Asp^{41}, respectively. Most important, Arg^{33} is replaced by a negatively charged aspartic acid at the tip of the second loop. Arg^{33} is one of the most critical residues, and its replacement by glutamic acid results in >300- and 750-fold decreases in binding affinity in erabutoxin-a (60, 61) and α-cobratoxin (53), respectively. Apart from common core residues, erabutoxin-a utilizes specific determinants crucial for *Torpedo* receptor recognition: Gln^7, Ser^8, Gln^{10}, Ile^{36}, and Glu^{38}. In denmotoxin, these residues correspond to Asn^{14}, Arg^{15}, Ser^{19}, Trp^{48}, and Val^{50}, respectively. It is not clear how denmotoxin retains significant neurotoxicity (only a 10-fold loss compared with α-bungarotoxin) even though most of the functional residues are replaced. It is possible that denmotoxin binds to nAChRs utilizing other residues that have yet to be identified.

Some 3FTXs bind to their receptors virtually irreversibly, whereas others exhibit reversible binding (18, 62, 63), and the molecular determinants that contribute to reversibility are not known. However, it has been reported that mutation of a single amino acid residue (Phe^{38} to Ile) in the muscarinic 3FTX m1-toxin1 (*Dendroaspis angusticeps*) changes toxin binding to the M_1 muscarinic receptor from irreversible to completely reversible (64). As shown here, the neuromuscular blockage of chick nerve-muscle junctions by denmotoxin is irreversible. α-Colubritoxin (from *C. radiatus* venom), which shows ~50% sequence identity to denmotoxin, exhibits a potent postsynaptic effect and completely inhibits indirect twitches in CBCM in 30 min (1 μM), but this blockage is reversible (18). Structure-function relationships of these two toxins may help us to delineate the residues involved in their reversible/irreversible binding. The physiological relevance of such reversibility of binding is not clear but may result from selection for specific structural variants of 3FTXs with taxon-specific effects (49).

During the evolution of nAChRs, residues critical for α-neurotoxin binding (65, 66) have been highly conserved in various taxa (from fishes to mammals), but in resistant organisms, this region has often been significantly modified. Some of the species-specific susceptibility/resistance to postsynaptic neurotoxins is correlated with a substitution of residues leading to additional *N*-glycosylation sites near the ligand-binding site in the nAChR (67, 68). A functional result of this modification is that the motor end plate nAChRs of many snakes and mammals such as the mongoose are much less sensitive to postsynaptic neurotoxins (69, 70). Comparative sequence analysis of nAChRs from mouse, mongoose, and snake shows mutations of W187N in mongoose (67) and F189N in snake (68). These additional *N*-glycosylation sites confer a barrier to the toxin, allowing access for small ligands

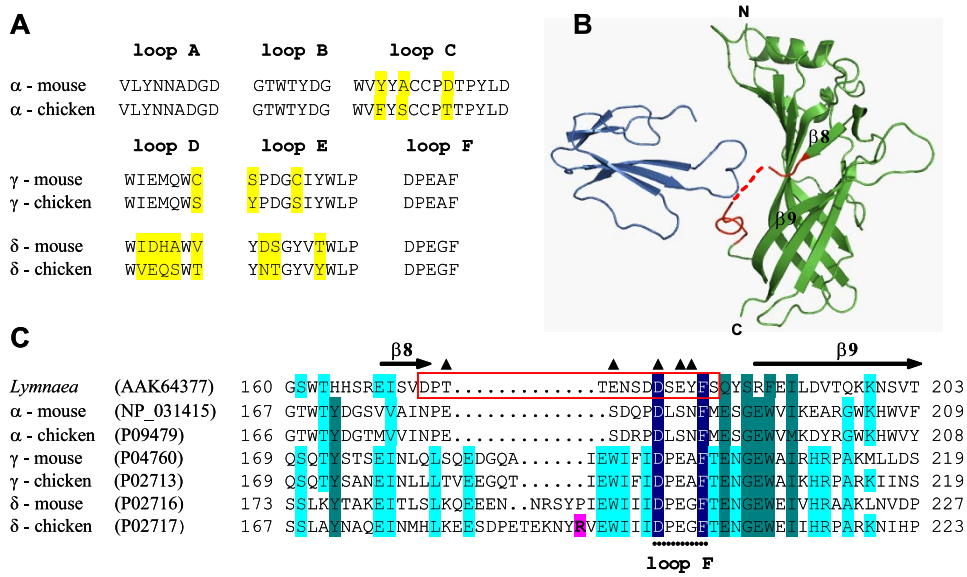

FIGURE 6. **Interaction sites between nAChRs and postsynaptic neurotoxin.** *A*, pairwise sequence alignment of the functional loops of the α_1-, γ-, and δ-subunits of mouse and chick muscle nAChRs. Loops A–C belong to the α-subunit and constitute the principal component of the plus side of the ligand-binding site interface. Loops D–F (γ- and δ-subunits) belong to the complementary component at the minus side of the interface of the ligand-binding site. Non-identical residues are shown in *yellow*. *B*, α-cobratoxin (*blue*) interaction with the complementary face of the AChBP subunit (*green*) (59). The segment that forms the part of the complementary face between β8 and β9 of AChBP is colored *red*. The *dashed line* indicates the disordered region in the structure. *C*, partial sequence of the *L. stagnalis* AChBP subunit aligned with equivalent regions of the α-, γ-, and δ-subunits of chick and mouse muscle nAChRs. The source of each sequence (Swiss-Prot accession number) is given in *parentheses*. The residues that have 100, ≥75, and ≥50% identity are colored in *dark blue*, *marine blue*, and *light blue*, respectively. The secondary structural elements (β8 and β9) are shown according to the crystal structure of *L. stagnalis* AChBP (PDB code 1UX2). *Triangles* denote AChBP residues from the complementary faces of the subunit interface that interact with α-cobratoxin (59). Arg^{193}, which may contribute to the bird specificity of denmotoxin, is highlighted in *red* (for details, see "Discussion"). The *red box* indicates AChBP residues (Asp^{172}–Ser^{185}) colored in *red* in *B*.

such as acetylcholine. We compared the amino acid sequences of chick (α, Swiss-Prot accession number P09479; β, accession number P16005; γ, accession number P02713; and δ, accession number P02717) and mouse (α, accession number NP_031415; β, accession number P09690; γ, accession number P04760; and δ, accession number P02716) $\alpha_1\beta\gamma\delta$-nAChRs. They show high sequence identity overall as well as within functional loops. There is no difference in *N*-glycosylation pattern between the chick and mouse receptors. Thus, the reversibility and resistance of mouse nAChRs to denmotoxin do not appear to be related to the differences in glycosylation. As the tip of the central loop of denmotoxin is negatively charged, in contrast to the positively charged tip in postsynaptic neurotoxins (Asp^{41} in denmotoxin *versus* Arg^{33} in erabutoxin-a and α-cobratoxin), we focused on substitutions leading to charge changes in the regions with close proximity to the toxin-binding site in the mouse and chick $\alpha_1\beta\gamma\delta$-nAChRs. Functional loops A and B from the α-subunit and loops F from the γ- and δ-subunits are identical in both species (Fig. 6*A*). In loop C (α-subunit) and loops D and E (γ- and δ-subunits), there are several amino acid replacements compared with the sequences of both nAChRs (Fig. 6*A*), which may contribute to species-dependent receptor susceptibility to denmotoxin. However, in these segments, none of the substitutions led to an increase in positive charge in the chick receptor compared with the mouse receptor, which could explain the taxon-specific binding of denmotoxin. Recently, AChBP from *Lymnaea stagnalis*, a homolog of the N-terminal ligand-binding domain of nAChRs, has been co-crystallized with α-cobratoxin (PDB code 1UX2) (59). The complex structure reveals toxin-receptor interactions. There is an unstructured region between β8 and β9 (Fig. 6, *B* and *C*) that is involved in the interaction. This segment is considered to be equivalent to the complementary face of the γ- and δ-subunits of muscle nAChRs. Unlike in the mouse $\alpha_1\beta\gamma\delta$-nAChR, Arg^{193} is in the δ-subunit of the chick $\alpha_1\beta\gamma\delta$-nAChR in this region, just in front of functional loop F (Fig. 6*C*). Arg^{193} may contribute to electrostatic interactions with denmotoxin Asp^{41}, causing an enhanced and irreversible binding of the toxin to the chick $\alpha_1\beta\gamma\delta$-nAChR. Thus, Arg^{193} in the chick δ-subunit may explain the observed species specificity. However, toxin-receptor interactions are likely complex, and additional studies (*e.g.* double cycle mutant experiments with chick and mouse $\alpha_1\beta\gamma\delta$-nAChRs) are needed to elucidate the relative importance of residue substitutions.

CONCLUSION

We have identified, purified, and characterized a novel toxin (denmotoxin) from the venom of the colubrid snake *B. dendrophila.* It exhibits taxon-specific postsynaptic neuromuscular blockage and potently and irreversibly blocks chick neuromuscular transmission but weakly and reversibly blocks mouse neuromuscular transmission. Crystallographic determination of the three-dimensional structure of this unique 3FTX, which possesses an N-terminal extension, showed that the characteristic structural motif of the 3FTXs is conserved. The structural and functional characterizations of this colubrid non-conventional 3FTX will provide the foundation for a better understanding of the species specificity and reversibility of postsynaptic neurotoxins.

Acknowledgments—We thank Shoon Mei Leng for invaluable help, assistance, and technical advice during organ bath experiments; William H. Heyborne for assistance with venom extractions; and Dr. S. Jayaraman for help in the final structure refinement.

REFERENCES

1. Endo, T., and Tamiya, N. (1987) *Pharmacol. Ther.* **34,** 403–451
2. Kini, R. M. (2002) *Clin. Exp. Pharmacol. Physiol.* **29,** 815–822

3. Nirthanan, S., Gopalakrishnakone, P., Gwee, M. C., Khoo, H. E., and Kini, R. M. (2003) *Toxicon* **41,** 397–407
4. Servent, D., and Ménez, A. (2001) in *Handbook of Neurotoxicology* (Massaro, E. J., ed) pp. 385–425, Human Press, Totowa, NY
5. Tsetlin, V. (1999) *Eur. J. Biochem.* **264,** 281–286
6. Ricciardi, A., Le Du, M. H., Khayati, M., Dajas, F., Boulain, J. C., Ménez, A., and Ducancel, F. (2000) *J. Biol. Chem.* **275,** 18302–18310
7. Ohno, M., Ménez, R., Ogawa, T., Danse, J. M., Shimohigashi, Y., Fromen, C., Ducancel, F., Zinn-Justin, S., Le Du, M. H., Boulain, J. C., Tamiya, T., and Ménez, A. (1998) *Prog. Nucleic Acid Res. Mol. Biol.* **59,** 307–364
8. Potter, L. T. (2001) *Life Sci.* **68,** 2541–2547
9. Yasuda, O., Morimoto, S., Jiang, B., Kuroda, H., Kimura, T., Sakakibara, S., Fukuo, K., Chen, S., Tamatani, M., and Ogihara, T. (1994) *Artery* **21,** 287–302
10. De Weille, J. R., Schweitz, H., Maes, P., Tartar, A., and Lazdunski, M. (1991) *Proc. Natl. Acad. Sci. U. S. A.* **88,** 2437–2440
11. McDowell, R. S., Dennis, M. S., Louie, A., Shuster, M., Mulkerrin, M. G., and Lazarus, R. A. (1992) *Biochemistry* **31,** 4766–4772
12. Williams, J. A., Lu, X., Rahman, S., Keating, C., and Kakkar, V. (1993) *Biochem. Soc. Trans.* **21,** 73S
13. Wu, P. L., Lee, S. C., Chuang, C. C., Mori, S., Akakura, N., Wu, W. G., and Takada, Y. (2006) *J. Biol. Chem.* **281,** 7937–7945
14. Karlsson, E., Mbugua, P. M., and Rodriguez-Ithurralde, D. (1984) *J. Physiol.* (*Paris*) **79,** 232–240
15. Kumar, T. K., Jayaraman, G., Lee, C. S., Arunkumar, A. I., Sivaraman, T., Samuel, D., and Yu, C. (1997) *J. Biomol. Struct. Dyn.* **15,** 431–463
16. Banerjee, Y., Mizuguchi, J., Iwanaga, S., and Kini, R. M. (2005) *J. Biol. Chem.* **280,** 42601–42611; Correction (2006) *J. Biol. Chem.* **281,** 22427
17. Chang, C. C. (1999) *J. Biomed. Sci.* **6,** 368–375
18. Fry, B. G., Lumsden, N. G., Wuster, W., Wickramaratna, J. C., Hodgson, W. C., and Kini, R. M. (2003) *J. Mol. Evol.* **57,** 446–452
19. Vidal, N., and Hedges, S. B. (2002) *C. R. Biol.* **325,** 987–995
20. Vidal, N., and Hedges, S. B. (2005) *C. R. Biol.* **328,** 1000–1008
21. Hill, R. E., and Mackessy, S. P. (2000) *Toxicon* **38,** 1663–1687
22. Mackessy, S. P. (2002) *J. Toxicol. Toxin Rev.* **21,** 43–83
23. Hill, R. E., and Mackessy, S. P. (1997) *Toxicon* **35,** 671–678
24. Chang, C. C., and Lee, C. Y. (1963) *Arch. Int. Pharmacodyn. Ther.* **144,** 241–257
25. Fry, B. G., Wuster, W., Ramjan, S. F. R., Jackson, T., Martelli, P., and Kini, R. M. (2003) *Rapid Commun. Mass Spectrom.* **17,** 2047–2062
26. Mourier, G., Servent, D., Zinn-Justin, S., and Ménez, A. (2000) *Protein Eng.* **13,** 217–225
27. Wang, S. S. (1973) *J. Am. Chem. Soc.* **95,** 1328–1333
28. Mourier, G., Dutertre, S., Fruchart-Gaillard, C., Ménez, A., and Servent, D. (2003) *Mol. Pharmacol.* **63,** 26–35
29. Gilsborg, B. L., and Warriner, J. (1960) *Br. J. Pharmacol. Chemother.* **15,** 410–411
30. Bulbring, E. (1997) *Br. J. Pharmacol.* **120,** 3–26
31. Otwinowski, Z., and Minor, W. (1997) *Methods Enzymol.* **276,** 307–326
32. Vagin, A., and Teplyakov, A. (1997) *J. Appl. Crystallogr.* **30,** 1022–1025
33. Murshudov, G. N., Vagin, A. A., and Dodson, E. J. (1997) *Acta Crystallogr. Sect. D Biol. Crystallogr.* **53,** 240–255
34. Brunger, A. T., Adams, P. D., Clore, G. M., DeLano, W. L., Gros, P., Grosse-Kunstleve, R. W., Jiang, J. S., Kuszewski, J., Nilges, M., Pannu, N. S., Read, R. J., Rice, L. M., Simonson, T., and Warren, G. L. (1998) *Acta Crystallogr. Sect. D Biol. Crystallogr.* **54,** 905–921
35. Laskowski, R. A., MacArthur, M. W., Moss, D. S., and Thornton, J. M. (1993) *J. Appl. Crystallogr.* **26,** 283–291
36. Holm, L., and Sander, C. (1995) *Trends Biochem. Sci.* **20,** 478–480
37. Lewis, R. J., and Garcia, M. L. (2003) *Nat. Rev. Drug Discov.* **2,** 790–802
38. Smith, C. G., and Vane, J. R. (2003) *FASEB J.* **17,** 788–789
39. Fiordalisi, J. J., al Rabiee, R., Chiappinelli, V. A., and Grant, G. A. (1994) *Biochemistry* **33,** 12962–12967
40. Levinson, S. R., Evans, M. H., and Groves, F. (1976) *Toxicon* **14,** 307–312
41. Weinstein, S. A., Chiszar, D., Bell, R. C., and Smith, L. A. (1991) *Toxicon* **29,** 401–407
42. Broaders, M., Faro, C., and Ryan, M. F. (1999) *J. Nat. Toxins* **8,** 155–166
43. Lumsden, N. G., Fry, B. G., Kini, R. M., and Hodgson, W. C. (2004) *Toxicon* **43,** 819–827
44. Lumsden, N. G., Fry, B. G., Ventura, S., Kini, R. M., and Hodgson, W. C. (2004) *Auton. Autacoid Pharmacol.* **24,** 107–113
45. Lumsden, N. G., Fry, B. G., Ventura, S., Kini, R. M., and Hodgson, W. C. (2005) *Toxicon* **45,** 329–334
46. Brazil, V., and Vellard, J. (1926) *Mem. Inst. Butantan* **3,** 301–325
47. Martins, N. (1917) *Collect. Trab. Inst. Butantan 1907–1917* **1,** 427–496
48. Prado-Franceschi, J., Hyslop, S., Cogo, J. C., Andrade, A. L., Assakura, M., Cruz-Hofling, M. A., and Rodrigues-Simioni, L. (1996) *Toxicon* **34,** 459–466
49. Mackessy, S. P., Sixberry, N. M., Heyborne, W. H., and Fritts, T. (2006) *Toxicon* **47,** 537–548
50. Ménez, A., Bouet, F., Guschlbauer, W., and Fromageot, P. (1980) *Biochemistry* **19,** 4166–4172
51. Endo, T., and Tamiya, N. (1991) in *Snake Toxins* (Harvey, A. L., ed) pp. 165–222, Pergamon Press, New York
52. Dufton, M. J., and Hider, R. C. (1988) *Pharmacol. Ther.* **36,** 1–40
53. Antil, S., Servent, D., and Ménez, A. (1999) *J. Biol. Chem.* **274,** 34851–34858
54. Torres, A. M., Kini, R. M., Selvanayagam, N., and Kuchel, P. W. (2001) *Biochem. J.* **360,** 539–548
55. Ackermann, E. J., Ang, E. T., Kanter, J. R., Tsigelny, I., and Taylor, P. (1998) *J. Biol. Chem.* **273,** 10958–10964
56. Osaka, H., Malany, S., Molles, B. E., Sine, S. M., and Taylor, P. (2000) *J. Biol. Chem.* **275,** 5478–5484
57. Malany, S., Osaka, H., Sine, S. M., and Taylor, P. (2000) *Biochemistry* **39,** 15388–15398
58. Teixeira-Clerc, F., Ménez, A., and Kessler, P. (2002) *J. Biol. Chem.* **277,** 25741–25747
59. Bourne, Y., Talley, T. T., Hansen, S. B., Taylor, P., and Marchot, P. (2005) *EMBO J.* **24,** 1512–1522
60. Pillet, L., Tremeau, O., Ducancel, F., Drevet, P., Zinn-Justin, S., Pinkasfeld, S., Boulain, J. C., and Ménez, A. (1993) *J. Biol. Chem.* **268,** 909–916
61. Tremeau, O., Lemaire, C., Drevet, P., Pinkasfeld, S., Ducancel, F., Boulain, J. C., and Ménez, A. (1995) *J. Biol. Chem.* **270,** 9362–9369
62. Nirthanan, S., Charpantier, E., Gopalakrishnakone, P., Gwee, M. C., Khoo, H. E., Cheah, L. S., Bertrand, D., and Kini, R. M. (2002) *J. Biol. Chem.* **277,** 17811–17820
63. Harvey, A. L., and Rodger, I. W. (1978) *Toxicon* **16,** 219–225
64. Krajewski, J. L., Dickerson, I. M., and Potter, L. T. (2001) *Mol. Pharmacol.* **60,** 725–731
65. Grutter, T., and Changeux, J. P. (2001) *Trends Biochem. Sci.* **26,** 459–463
66. Fruchart-Gaillard, C., Gilquin, B., Antil-Delbeke, S., Le Novere, N., Tamiya, T., Corringer, P. J., Changeux, J. P., Ménez, A., and Servent, D. (2002) *Proc. Natl. Acad. Sci. U. S. A.* **99,** 3216–3221
67. Barchan, D., Kachalsky, S., Neumann, D., Vogel, Z., Ovadia, M., Kochva, E., and Fuchs, S. (1992) *Proc. Natl. Acad. Sci. U. S. A.* **89,** 7717–7721
68. Takacs, Z., Wilhelmsen, K. C., and Sorota, S. (2001) *Mol. Biol. Evol.* **18,** 1800–1809
69. Neumann, D., Barchan, D., Horowitz, M., Kochva, E., and Fuchs, S. (1989) *Proc. Natl. Acad. Sci. U. S. A.* **86,** 7255–7259
70. Burden, S. J., Hartzell, H. C., and Yoshikami, D. (1975) *Proc. Natl. Acad. Sci. U. S. A.* **72,** 3245–3249